

# Unmanned Aerial Auger for Underground Sensor Installation

Yue Sun, Adam Plowcha, Mark Nail, Sebastian Elbaum, Benjamin Terry, and Carrick Detweiler

**Abstract**—Using an Unmanned Aerial Systems (UAS) to autonomously deploy soil sensors enables their installation in otherwise hard to access locations. In this paper, we present a system that integrates a UAS and a digging mechanism which can carry, secure, and install a small sensor into dirt effectively and efficiently. The integrated system includes 1) a low profile, light-weight, inexpensive auger mechanism, 2) a sensor carrying and deploying mechanism with low power consumption, and 3) sensors and software that control and evaluate the auger performance during digging. When tested on a suite of target soils and a target depth of 120mm, the system achieved a success rate of 100% for indoor tests and 92.5% for outdoors, verifying the potential of the approach.

## I. INTRODUCTION

Unmanned Aerial Systems (UAS) are commonly used to facilitate data collection in a wide range of applications. The most popular modality consists of equipping the system with on-board sensors such as cameras and laser scanners for remote sensing. UASs can also be used to collect data from sensors deployed in the field that require longer deployments or that cannot be carried by the UAS [1]. A third and less explored modality consists of utilizing the UAS to actually deploy sensors in locations that are challenging to reach by other means [2]. This third modality is particularly challenging when the sensor placement has special requirements in terms of position, location, and general manipulation.

In this work we develop a system and experimentally verify the performance of a UAS that can carry a sensor and insert it into the soil via an auger mechanism. Placement of sensors underground requires that the UAS is able to identify the proper target location, break the ground surface, remove the soil, and correctly place the sensor. A significant challenge is how to perform these tasks successfully within the weight and power constraints of a UAS.

Our key contribution is the development and assessment of an autonomous aerial auger for sensor deployment, shown in Fig. 1. The system is capable of securely carrying a sensor the size of a soda-can and installing it at various depths up to 250mm. The whole system weights less than 1200 grams to fit within the weight constraints of many small commercial UASs, yet it includes many features to support successful sensor placement such as the feedback mechanisms to detect

Y. Sun, M. Nail and B. Terry are with the Department of Mechanical Engineering, University of Nebraska-Lincoln, Lincoln, NE 68588, USA [bterry2@mme.unl.edu](mailto:bterry2@mme.unl.edu), [mnail@mme.unl.edu](mailto:mnail@mme.unl.edu), [ysun@mme.unl.edu](mailto:ysun@mme.unl.edu)

A. Plowcha, S. Elbaum, and C. Detweiler are with the Department of Computer Science and Engineering, University of Nebraska-Lincoln, Lincoln, NE 68588, USA [carrick@cse.unl.edu](mailto:carrick@cse.unl.edu), [elbaum@cse.unl.edu](mailto:elbaum@cse.unl.edu), [pplowcha@cse.unl.edu](mailto:pplowcha@cse.unl.edu)

This material is based upon work supported by USSTRATCOM through the 55th Contracting Squadron under Contract No. FA4600-12-D-9000 and was also funded, in part, by NSF-1638099 and USDA-2017-67021-25924.



Fig. 1: The unmanned aerial auger in flight.

when the installation is not successful and must be either retrieved at a different location, or aborted by sacrificing the sensor in order to save the UAS.

We analyzed the system performance on a target soil using a cutting bit that was optimized for that soil type. Indoor tests resulted in a success rate of 100% for deploying sensor into silty-sand at target depths between 120 to 250 mm. Outdoor experiments showed a 92.5% success of the complete system on the target soil, with the two failures caused by a poor landing and by a released sensor that did not stay completely in the dug hole when the UAS departed. We also analyzed the system robustness to soil variation, and explored how the system sensor readings must be interpreted and how the system parameters may be adjusted to improve the overall performance.

## II. RELATED WORK

There is a wide range of work related to UAS based ground sensing that can be classified in two main categories: (1) ground surface classification, and (2) underground monitoring.

Within ground surface classification, both remote sensing strategies and physical contact methods have been implemented with UAS to classify surface types. Thrun et al. use a helicopter equipped with a laser-scanner to build a three dimensional map of environment [9]. Templeton et al. use a vision system to distinguish safe landing areas [10]. In our previous work, we used accelerometer data of the UAS from a single landing to accurately classify the softness of the surface with 90% accuracy [2]. We are continuing that work by developing a UAS capable of contributing to an underground monitoring system.

UAS-based underground monitoring mainly relies on deployed sensors below the ground surface. Corke et al. use an autonomous helicopter to deploy a sensor network for

	Drilling Strategy	Propulsive Force	Substrate Type	Diameter (mm)	Max.Depth (mm)	Weight (g)	Power (w)
CSD [3]	Rotary	Self-weight	Soil	50	1000	604	23.8
SPA [4]	Hammer-Rotary	Impact Force	Rock,Soil	10	80(rock)	1814	100
PLUTO [5]	Hammer	Impact Force	Soil	20	600	900	5
DRD [6]	Bio-inspired	Extra Weight	Soil	50	1000	2700	3
MMUM [7]	Hammer	Impact Force	Soil	40	2000	2000	10
USDC [8]	Hammer	Impact Force	Rock,Soil	3	1760	450	10

TABLE I: Conventional digging mechanisms.

monitoring [11]. Sensors were dropped to the ground through a wire coil one at a time when a radio controlled servo rotated a certain number of rotations. Anthony et al. used UAS to insert a soil moisture probe into ground to monitor soil conditions [2]. Pister et al. use a fixed-wing UAS to build a ground sensor network to track vehicles [12]. Sensors were deployed through a custom dropper. None of the above methods dig into the ground to deploy a sensor completely below ground surface.

*To our knowledge, this project is the first one using UASs for remote sensor installation with depth requirements to form an underground monitoring system.* To reach target depth, an appropriate digging mechanism must not only be able to penetrate into the ground to install a sensor, but also must meet the weight, power, and size constraints of UASs. In this section we continue to discuss multiple related digging mechanisms that have potential to be implemented with UASs.

Diggers can be classified into three types: rotary drilling, hammer drilling, and rotary-hammer drilling [13] [14]. Rotary drills are the most commonly used mechanisms for subsurface access, consisting of a cutting bit for breaking through substrates and a conveyor mechanism for transporting the cut material back to the surface. For example, a coaxial double rotary screw penetrator, named Contra-rotor Screw Drill, was designed to penetrate into substrates with minimal reaction force [3]. Hammer drills use impact force to crack and compact substrates and are good at penetrating brittle and soft materials. It is the most popular strategy used to explore on extraterrestrial planets. Several surface sampling devices, like the PLUTO (Planetary Underground Tool) Mole Sampling Device on the Europe Space Agency Mars Express lander Beagle 2 [5], the Moon/Mars Underground Mole (MMUM) planetary subsurface sampling device [7] and Ultrasonic/Sonic Driller/Corer [8] from NASA JPL use internal percussive actions with various frequencies to propel themselves into substrates. Rotary-hammer drills operate percussively on objects, introducing impact forces, while at the same time rotating the cutting bit to break through the substrates. For instance, a compact and lightweight drill that uses a single piezoelectric actuator (SPA) to produce both hammering and rotation of the drill bit from JPL demonstrates satisfying digging performance on hard substrates [4]. Similarly, biologically inspired drilling mechanisms that mimic the penetration movements of insects also utilize such hybrid designs [6]. Table I presents a comparison between these technologies.

### III. SYSTEM REQUIREMENTS

At the most general level, the unmanned aerial auger system must be able to reach a target location while carrying a sensor, place the sensor at a specified depth, and return home. This general requirement can be tailored for specific contexts by adjusting three parameters: sensor type, soil type, and target distance. Without loss of generality for the context of this paper, we are aiming to place underground moisture sensors to characterize water absorption and retention in a diverse landscape covering hundreds of acres. Hence, our tailoring of the three parameters is as follows:

- 1) **Sensor Type:** Soil moisture sensor with a battery and radio, as shown in Fig. 3c. The sensor shown here is customized to collect as well as transmit soil moisture data. It is 25 mm in diameter by 76 mm in length. Any type of commercial sensor with equal or smaller dimensions can also be carried and installed by our system.
- 2) **Soil Type:** Silty-sand, which consists of silt and sand with different percentages by weight. More specifics about this type of soil and a wider range of soils is presented in Section IV-C.
- 3) **Distance to target area:** We are aiming to place a sensor within a mile of the ground station.

Defining these three key parameters has implications for the selection of the UAS and the design of the digging system. **UAS selection:** For our study we selected a DJI Matrice 100 quadrotor, due to its ability to meet our range and payload requirements while still being portable enough for a single individual to carry into the field.

**Digging depth:** 120 mm depth is needed for the soil moisture sensor to collect in-situ data on the target soil type. Achieving that depth implies generating enough downward force for a cutting bit to penetrate the ground (this force is also known as Weight on Bit (WOB), a crucial digging effectiveness measure).

**Sensor protection:** Since an exposed sensor might be damaged during digging, which is a hazardous process involving percussion and grinding, the sensor must be isolated and secured before deployment.

**Operating on uneven surfaces:** The system will be used outdoors on uneven surfaces so it must be able to land on uneven ground surfaces of up to 10 degrees.

**Sensor placement:** The sensor must be placed at the target depth with a maximum tilt digging angle of 10 degrees. Partially exposed sensors are not effective and must be removed.

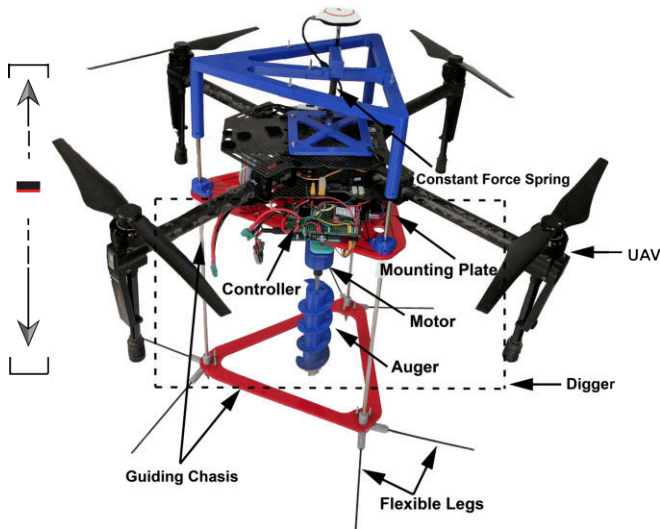


Fig. 2: System overview.

**Return to base:** The system must fly back to the launch point where the operator can reload a new sensor to start another mission. This implies that the system must not become stuck while digging.

**Digging speed:** For our current scenario speed is not a concern, our focus is exclusively on depth.

#### IV. SYSTEM DESIGN

The system design overview is shown in Fig. 2. We will now discuss its different components considering the mechanical, electrical, and computational design.

##### A. Mechanical Design

The mechanical system is composed of three main parts: the sensor locking and releasing mechanism displayed in Fig. 3a, the integration of the UAS and the auger presented in Fig. 3b, and the cutting bit and a screw conveyor shown in Fig. 3c. The mass of the system that attached to the UAS is 1.2 kg. The overall length of the integrated system is 540 mm while the distance for the auger to slide is 380 mm.

**Sensor carry and release mechanism:** To carry, secure, and release the sensor, we developed an active locking and release mechanism integrated with the auger as shown in Fig. 3a. It consists of two parts, which are the key connected to the motor shaft and the key lock mechanism attached to the top of the auger. The inner area of the screw conveyor is hollow to contain the sensor electronics. At the beginning of each mission, the sensor is manually slid into the hollow area and the cutting tip is fixed to the screw conveyor by two screws. By doing this, the sensor is isolated and secured properly during flying and augering operations. Then, the complete system is ready to takeoff after manually setting the key to position 1. When arriving at the target location, the key is pushed to position 2 due to the downward landing force from the UAS. The motor drives the auger to rotate clockwise through the key which stays at position 2. After achieving the target depth, the key is rotated counter-clockwise to arrive

at position 3, which is the open area between position 2 and 4. This allows the UAS to fly away while the sensor and auger remain in the ground. Position 4 is used for counter-clockwise rotation to reverse the auger bit in the event of a failed digging attempt so that the UAS can fly to a new location and try again. When digging resumes, the key moves back to position 2.

**Digger and UAS integration:** The larger the downward axial pushing force, the deeper the digger can reach. Thus, we must provide as much downward axial force as possible to reach the target digging depth. This idea drives the design of the integration between the digger and the UAS.

The downward axial force is obtained from two sources: the weight of the digging mechanism itself and the weight of the UAS. We attached the auger to the bottom of the UAS by a middle mounting plate, as shown in Fig. 3b. These two are regarded as one integrated part that slide together along the steel guiding rods during digging. It also connects to the top frame with constant force springs. The constant force spring allows the weight of the UAS to be divided into two portions: one portion is converted to the downward axial force to increase the value of WOB, which presses the cutting bit into the soil during digging. The other portion is transformed as the downward force exerted on the three spike-tipped legs to counter the torque created by the auger as it penetrates the soil.

As a result of this landing frame, the complete system is fixed on the ground and a larger downward axial force is exerted on the auger. The force on the auger can be adjusted by selecting different constant force springs. The key requirement is that there needs to be sufficient force on the legs to prevent the whole system from rotating when digging. The value of these two portions can be determined experimentally.

**Cutting Bit:** The cutting bit is the main driving part for soil penetration. To reach the target depth, it must keep breaking the substrate until it reaches the target depth. Since we are going to leave the bit and the sensor in the ground, we favored a disposable bit design. The main body of the cutting bit is 3D printed and the cutting edges are formed from sections of hacksaw blades, which are sharp and durable enough to keep cutting the soil during digging. Theoretically, the cutting performance depends mainly on two design specs: the cutting angle, which describes the angle between the cutting surface and the soil surface, and the length of cutting edges [15]. Since our cutting bit is small, we ignore the length of the cutting edges and only focus on the cutting angle determined experimentally in Section IV-C.

**Screw Conveyor:** The conveyor helps to transport cuttings back to ground surface and provides axial propulsive force. It is a cylinder winded by a helical flute, as shown in Fig. 3c. The design of a screw conveyor can be determined by six variables: the inner diameter, outer diameter, pitch, angle of helical flute, the width, and thickness of the flute [16]. Since the width of the flute is the distance between the inner diameter and the outer diameter, and there is a correlation between helix angle of the flute and pitch value

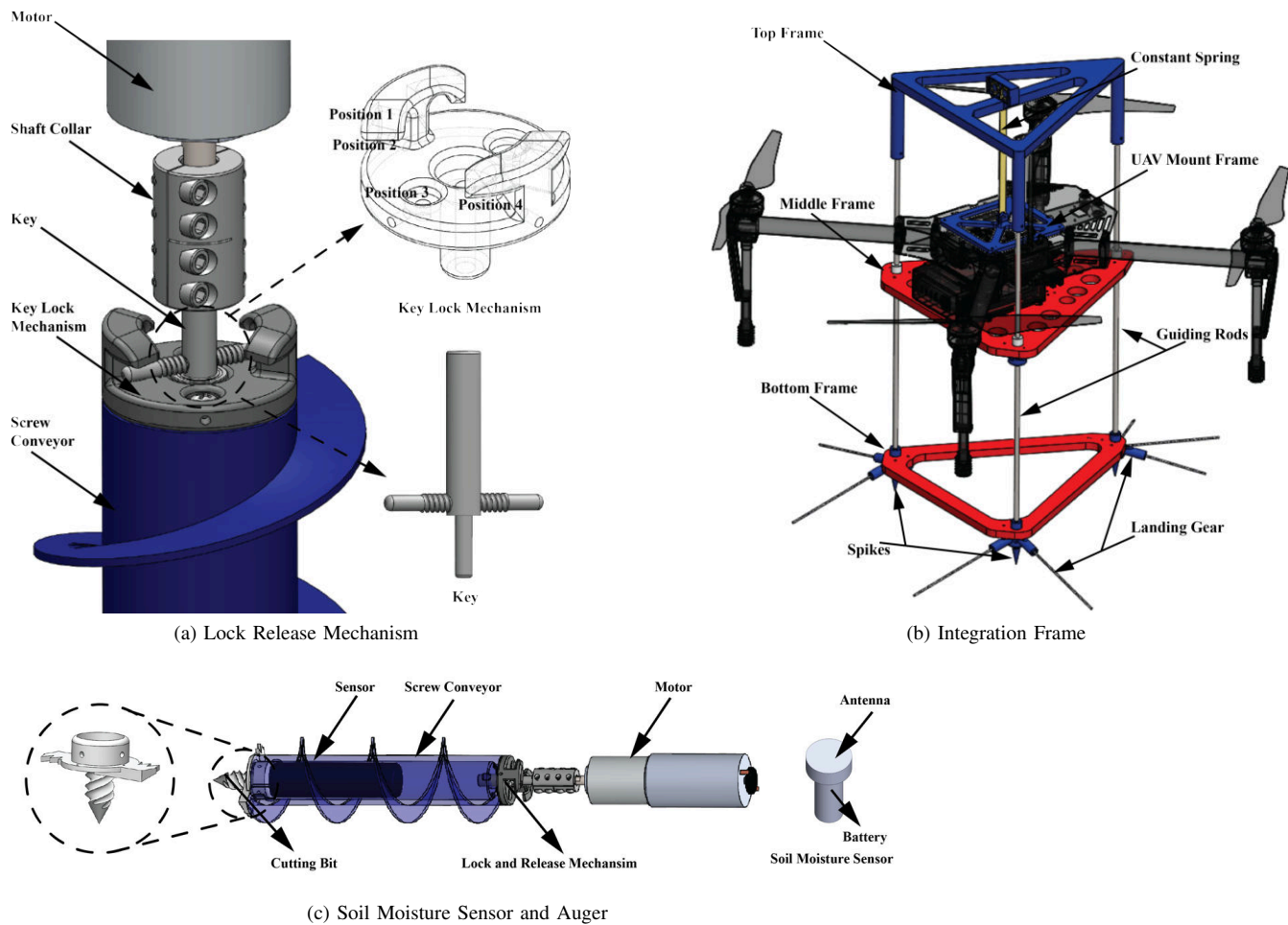


Fig. 3: Mechanical system details.

[17], those six variables can be combined into four. Due to the small size of the conveyor, the thickness of the flute will not significantly impact the transporting performance. We set the thickness of the flute to be 1.5 mm. The inner diameter of the conveyor is fixed based on the diameter of the sensor housed within the auger. As a result, there are only two variables left to finalize the design of our screw conveyor, which are the width,  $h$ , and helix angle,  $\alpha$ , of the flute. We experimentally determine the optimal values for those two parameters in Section IV-C. The landing gear of our system is shown in Fig. 3b. We added spikes to the bottom of the three legs to penetrate the soil and prevent the entire frame from twisting during digging operations. We also added two flexible outriggers to each of the three legs to aid with stability on landing.

### B. Electrical and Computing Design

The overall electrical and computing design involves a ground station, the UAS, and the digger as shown in Fig. 4. The ground station communicates with the UAS and the auger through separate channels, sending waypoints to the UAS and commands to the digger. Note that in the current design there is only a physical connection between the UAS

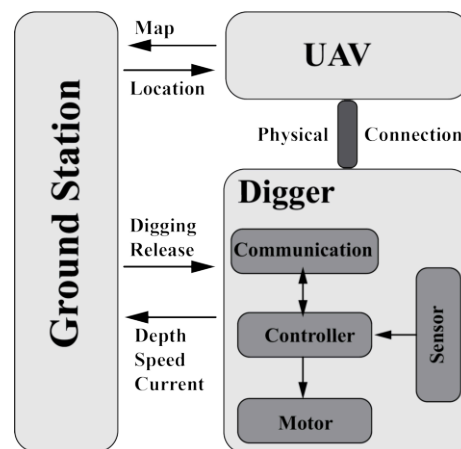


Fig. 4: System architecture.

and the digger which is meant to facilitate the transition of the auger to other UASs in the future.

Within the digger, the electrical and computing design was aimed at executing and assessing each sensor installation mission. This is accomplished by monitoring the motors, recording the real-time depth profile, controlling the

sequence of operations required to relocate the complete system to a new position to dig, or to release the sensor autonomously at desired depth.

The auger and the sensor locking and releasing mechanism are controlled by an ATmega328 microcontroller operating at 16 MHz with 2KB of SRAM and 32KB of flash memory. To ensure sufficient output torque before reach the target depth, we selected a planetary gear DC motor (Actobotics #638328) with gear ratio 27:1 to drive the auger. Its nominal voltage is 12V, no load speed is 313 RPM, stall current is 20 A and the maximum output torque is 2.9 N-m. The quadrature encoder on the motor is used to compute motor speed. A VNH3SP30 motor driver controls the rotary direction of the motor to dig, release the sensor, or reverse auger direction if needed. Current sensing is accomplished separately from the motor controller with an ACS715 0 to 30 A current sensor. The processor communicates to the ground station using a 2.4 GHz XBee Pro radio module that has a range of 1km. In order to have as much flight time as possible, the auger systems is powered by a single 11.1V 4900 mAh lithium polymer battery that is independent of the UAS power supply. A rotary quadrature encoder PEC11R was used to compute the digging depth. It is attached at the bottom of the middle plate, as shown in Fig. 5. Its shaft is rotated by a constant length cable fixed between the top frame and the bottom frame. The digging depth is proportional to the number of rotations of the rotary shaft.

During operation, the processor monitors the motor speed, motor current, and the digging depth. These parameters are transmitted from the auger to the ground station in real time and inform the operator about the digging performance of the auger. These parameters can be used to identify failure modes while digging. For instance, motor RPM that decreases toward zero and increasing current draw indicates the auger may be about to stop and that digging operations should cease to prevent motor overheating and damage. Conversely, if motor RPM remains high with relatively low current draw and no depth increase, then the auger is not making progress into the soil and digging should be attempted elsewhere. In either case, the auger can then be reversed and the UAS can fly to a new digging location to try again. The worst case scenario is if a stuck auger is unable to be rotated in either direction. In this case the key mechanism can still be moved to position 3 to abandon the sensor when only partially emplaced.

### C. Design Optimization

We conducted indoor tests with soil samples that matched the specifications given to us by our collaborators, and experimentally optimized our auger design for that specific soil. Our indoor testbed is shown in Fig. 5. The replicated silty-sand in the 300 mm diameter bucket consists of 20% clay and 80% sand by weight, and its preparation followed the standard Proctor test [18] to get a constant unconfined compressive strength value of 0.2Mpa [19]. The water content was set to be 10%. The dry bulk density was 1.79g/cc and wet bulk density was 1.99g/cc.

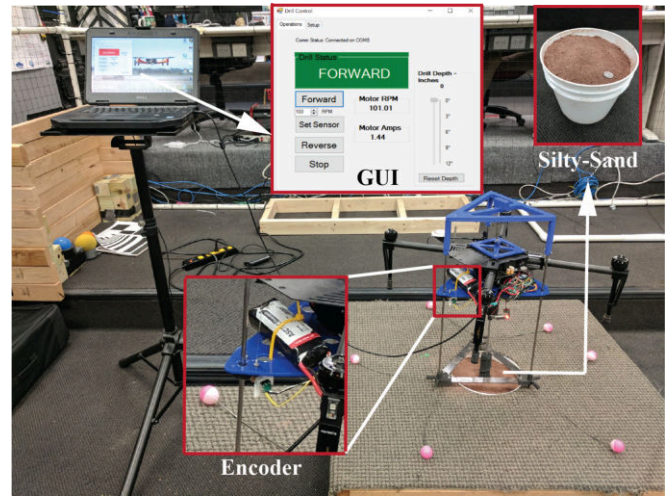


Fig. 5: Indoor testbed.



Fig. 6: Cutting bits.

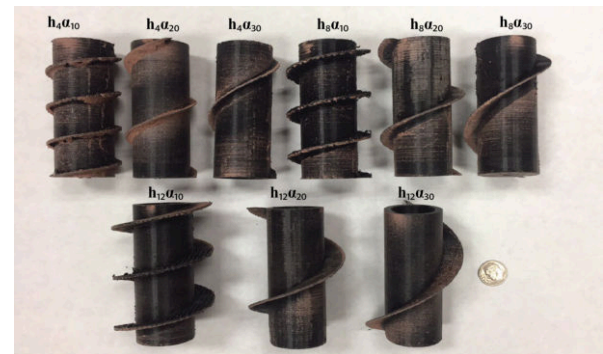


Fig. 7: Screw conveyors.

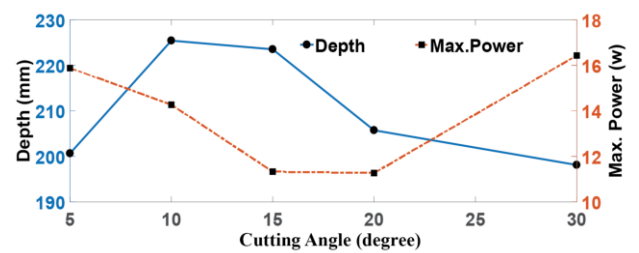


Fig. 8: Digging performance of different cutting bits.

We first evaluate the cutting angles' effect on digging performance by combining 5 different angles with same cutting blades, as shown in Fig. 6. For each trial, the WOB value was 9.8 N, which is the minimum required force we found to fix the complete system during digging process. The maximum depth allowed was 250 mm, and the cutting bit was attached to the same screw conveyor. Two outputs, depth

and maximum power, under varying cutting angles were recorded as shown in Fig. 8. Based on those two curves, the optimal value for cutting angle is 15 degrees as it minimizes power usage while maximizing depth.

Next, to find the best auger design, we evaluated the digging performance on the same soil by combining different screw conveyors with the cutting bit that has the cutting angle of 15 degrees. As discussed in Section IV, there are only two variables left (the width,  $h$ , and helix angle,  $\alpha$  of the flute) to finalize the design of screw conveyor. Based on the dimension of those existing compact screw conveyor for subsurface exploration [17] [20] [21], we select three width values: 4 mm, 8 mm, and 12 mm, and three helix angle values: 10-degree, 20-degree, and 30-degree to find best the combination for the given soil type, displayed in Fig. 7. The name of each width-helix angle combination is defined as  $h_i\alpha_j$ , where  $i$  and  $j$  are the values assigned to its corresponding variables. A total of 9 tests were conducted to find the best combination.

At the beginning of each test, we set the motor speed to 300rpm, which is the no-load speed of the motor we selected. We recorded depth profile, motor speed, and current. Depth profile is the most direct indicator showing the digging performance, and was used to calculate the rate of penetration. Motor current is used to find the power consumption of each digging attempt. The average current can also be indirectly used to calculate the output torque of the motor, which also helps with motor selection. The digging process was terminated when the auger kept spinning without gaining depth for 5 seconds (tip could not break the substrate) or when the digger got stuck and the current value spiked (clogged substrate does not move upwards).

To assess the performance of the 9 tests, we used three measures, shown in Table II. First, we measured the depth reached. Third, we collected the type of digging termination where “stuck” is an unacceptable outcome. Second, we measured the index of Specific Energy (SE), defined as the necessary mechanical energy to remove a unit volume of the substrates, it is a function of the digging diameter ( $D$ ), rotary speed ( $P$ ), rate of penetration (ROP), the weight of the digger itself ( $W_0$ ) and the external weight ( $W_1$ ) that is applied on the digger [22]. The lower the SE value, the better the digging performance [3]. Table II shows that  $h_{12}\alpha_{10}$  has the highest depth value and lowest SE value among those combinations whose termination type is “spinning”.

## V. FIELD STUDY

We conducted outdoor trials to assess the effectiveness of our complete system in the field. For all the outdoor trials, we manually navigated and landed the UAS. Future work will include making these functions autonomous. We defined a trial as successful if it can complete the following tasks: land at the target location, dig vertically (less than 10-degree), leave sensor between 120-250 mm underground, and fly back to the ground station where the operator can reload a sensor to start another mission. Fig. 9 displays a sequence of images of a successful sensor deployment.



(a) Take-off



(b) Landing



(c) Digging



(d) Sensor in Dirt

Fig. 9: A sequence of images of a complete successful trial.

### A. Setup

We prepared six target locations with different types of soil, including the target one at a farming site in Horning State Farm, NE. The soils were separated with wood plates, as shown in Fig. 10. The volume of each section was approximately 1 meter length by 1 meter width by 0.25 meter depth, and the condition of soil for each section is described in Table III.

We conducted 20 trials on the area filled with the target soil. The auger we used is the one which had the best indoor performance. The motor speed was set to be 300 rpm (maximum no load speed) before digging and the value of WOB was 1 kg (half weight of the UAS). Each trial was conducted with the same operational parameters.

We also conducted 10 trials on each of the other five soils utilizing the same digging procedure except that instead of flying back to the base at the end we manually lifted the UAS to accelerate the assessment process.

	$h_4\alpha_{10}$	$h_4\alpha_{20}$	$h_4\alpha_{30}$	$h_8\alpha_{10}$	$h_8\alpha_{20}$	$h_8\alpha_{30}$	$h_{12}\alpha_{10}$	$h_{12}\alpha_{20}$	$h_{12}\alpha_{30}$
Depth(mm)	196	177	112	198	263	81	<b>258</b>	223	149
SE(DJ/m <sup>3</sup> )	2.28	4.07	1.25	1.70	1.12	1.33	<b>1.35</b>	1.69	1.28
Type of Termination	spinning	spinning	stuck	spinning	stuck	stuck	<b>spinning</b>	spinning	stuck

TABLE II: The Results of the screw conveyor tests.

Soil Section	Soil Condition	Compaction (Mpa)	Water Content (%)
1	loose silty sand	$\leq 0.1$	4
2	compact silty sand ( <b>Target</b> )	0.2	12
3	compact silty sand	$\geq 0.45$	10
4	loose clay	0.15	3
5	moist&compact silty sand	0.15	16
6	moist&compact silty sand	$\geq 0.45$	21

TABLE III: Various soil types.

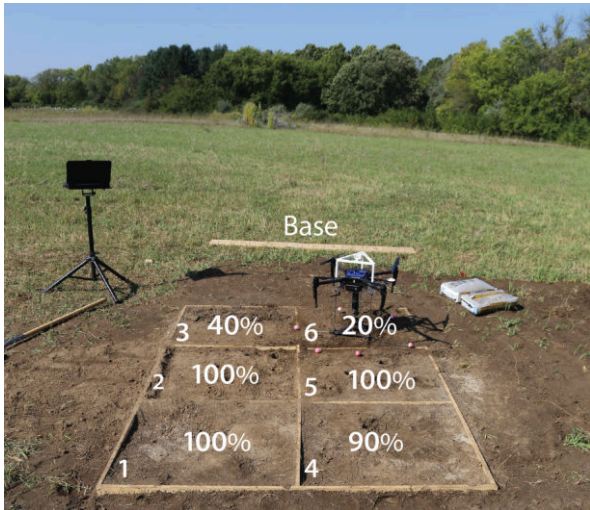


Fig. 10: Field testbed with six soil types (success percentage).

### B. Results on Target Soil

Table IV summarizes the outcomes of 20 trials on target soil section. Overall, 18 of the 20 trials were successful, and one was partially successful. The single failure occurred during the landing phase of the second trial as one of the legs hit an exposed wood frame during landing. For this trial we reset the UAS manually so that the rest of the trial could continue at that location but we still regarded the trial as a failure. In the ninth trial, the auger/sensor came part way out of the hole but then fell back in, which we counted as partially successful. The success rate of reaching the target depth, digging angle, and returning to base were 100%. The success rate of landing and sensor release was slightly lower. Overall, the success rate of our complete system on target soil is 92.5%.

### C. Results on All Soils

Table V shows the overall digging performance of our digger on various soil conditions. As expected, the digging difficulty increased as the compaction value and wetness increase. Our digger had almost 100% success on soil sections 1, 2 (target soil), 4 and 5, and much lower success

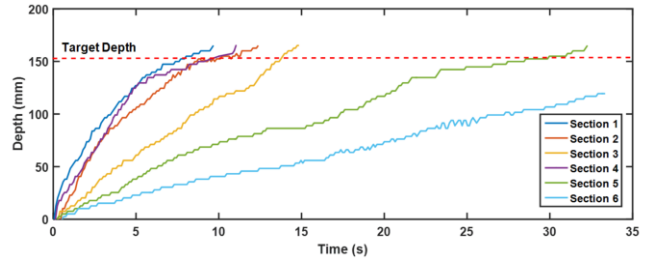


Fig. 11: Depth profile over 6 soil types.

rate on sections 3 and 6. As the wetness and compaction value of the soil increases, the auger tended to get stuck or spun without progress more often. Upon examination, we found that the digger failures were due in most cases to the moist clay lumped around the cutting bit jammed around the flutes prevent it from breaking through the soil. In fewer cases we found that the substrates were too hard for our cutting tip to breakthrough. For example, in one of the failures on soil section 3, the cutting tip was stuck in a soil layer filled with small gravel and grass roots 2 inches below the ground surface.

Fig. 10 describes the overall digging performance conducted in the six types of soil sections. Those success rates indicate that our auger can effectively perform sensor deployment mission on loose silt-sand, compacted silty-sand (unconfined stress value up to 0.2Mpa), loose clay and relatively low moisture silty-sand (water content up to 15%).

We note that all diggers, in some circumstances, may succeed even in the most challenging soils. Fig. 11 presents the depth profile of the trials with maximum digging depth on each of those six soil sections. The time to reach the target depth can vary by up to an order of magnitude depending on the soil type.

### D. Adjusting WOB for Soil Types

Since the auger system enables the quick adjustment of different WOB values, we performed additional experiments with increased WOB on the most challenging soil sections 3 and 6. We explored three new masses: 500grams, 1000grams and 1500grams, rendering WOB values of: 9.8N (W0), 14.7N (W1), 19.6N (W2), and 24.5N (W3). Following the same digging procedure previously defined while assuming the target location is already reached, we performed three trials on soil sections 3 and 6, for each of the three WOB values. A total of 18 trials were conducted.

As expected, the digging depth increased with an increase in WOB. For soil section 3, the average digging depth reached the target depth range when WOB value was set to equal or greater than W2. Similarly, the digging depth on

	Trials																				Success Rate
	1	2	3	4	5	6	7	8	9	10	11	12	13	14	15	16	17	18	19	20	
Landing	s	f	s	s	s	s	s	s	s	s	s	s	s	s	s	s	s	s	s	s	95%
Depth	s	s	s	s	s	s	s	s	s	s	s	s	s	s	s	s	s	s	s	s	100%
Sensor Release	s	s	s	s	s	s	s	s	ps	s	s	s	s	s	s	s	s	s	s	s	97.5%
Digging Angle	s	s	s	s	s	s	s	s	s	s	s	s	s	s	s	s	s	s	s	s	100%
Return to Base	s	s	s	s	s	s	s	s	s	s	s	s	s	s	s	s	s	s	s	s	100%
Overall Performance	s	f	s	s	s	s	s	s	ps	s	s	s	s	s	s	s	s	s	s	s	92.5%

s: success, f: failure, ps: is partial success.

TABLE IV: Field test evaluation table in target soil.

	Soil Section					
	1	2	3	4	5	6
Depth	s,s,s,s,s	s,s,s,s,s	s,f,f,f,f	s,s,s,s,s	s,s,s,s,s	s,f,s,f,f
Sensor Release	s,s,s,s,s	s,s,s,s,s	f,s,s,s,s	s,s,s,s,s	s,s,s,s,s	f,f,f,f,f
Digging Angle	s,s,s,s,s	s,s,s,s,s	f,s,s,s,s	s,s,s,s,s	s,s,s,s,s	s,s,s,s,s

s:success, f: failure.

TABLE V: Evaluation of digging on all soil sections.

soil section 6 increased to almost reach the minimum target depth with W3. We also found that the rate of penetration increased as the WOB increase. With W2, the maximum WOB value we can get from the selected UAS, the success rate of digging on soil section 3 increases from 20% to 40%. Simply selecting a heavier UAS may have proved sufficient for the system to succeed on all these soils.

## VI. CONCLUSION AND FUTURE WORK

We have shown a UAS-based auger system that can carry and deploy a sensor to a specific target depth in a column of soil. Our indoor and outdoor experiments showed the potential of the approach, its limitations, and several directions for improvement. First, we would like to close the loop between the navigation and the digging tasks. We are currently able to detect when the auger is struggling, but we have not yet linked that with navigation to identify more promising digging sites that may be in the proximity. Second, from a mechanical design perspective, although the current design is effective for placing one sensor, we would like to assess the possibility of being able to carry and deploy multiple sensors. Finally, the overall system effectiveness could dramatically increase if the system could tolerate landing at steeper angles and also be able to place the sensors at arbitrary angles that are independent of the slope.

## ACKNOWLEDGMENT

Thanks to Dr. Chung Song, Dr. Justin Bradley, Dr. Britany Duncan, Andrew Rasmussen, Ashraful Islam, Binyam Bekele, and the staff at Horning State Farm for their assistance.

## REFERENCES

- [1] M. Dunbabin and L. Marques, "Robots for environmental monitoring: Significant advancements and applications," *IEEE Robotics & Automation Magazine*, vol. 19, no. 1, pp. 24–39, 2012.
- [2] D. Anthony, E. Basha, J. Ostdiek, J. P. Ore, and C. Detweiler, "Surface classification for sensor deployment from uav landings," in *2015 IEEE International Conference on Robotics and Automation (ICRA)*, May 2015, pp. 3464–3470.
- [3] K. Nagaoka, T. Kubota, M. Otsuki, and S. Tanaka, "Experimental study on autonomous burrowing screw robot for subsurface exploration on the moon," in *Intelligent Robots and Systems, 2008. IROS 2008. IEEE/RSJ International Conference on*. IEEE, 2008, pp. 4104–4109.
- [4] S. Sherrit, L. Domm, X. Bao, Y. Bar-Cohen, Z. Chang, and M. Badescu, "Single piezo-actuator rotary-hammering (sparh) drill," 2012.
- [5] L. Richter, V. Gromov, H. Kochan, K. Kosacki, and T. Tokano, "The planetary underground tool (pluto) experiment on the beagle 2 mars lander," in *Sixth International Conference on Mars*, 2003.
- [6] Y. Gao, A. Ellery, M. Jaddou, J. Vincent, and S. Eckersley, "A novel penetration system for in situ astrobiological studies," *International Journal of Advanced Robotic Systems*, vol. 2, no. 4, p. 29, 2005.
- [7] C. Stoker, A. Gonzales, and J. Zavaleta, "Moon/mars underground mole," in *Proc. 2007 NASA Science Technology Conf*, vol. 6, 2007.
- [8] Y. Bar-Cohen, Z. Chang, S. Sherrit, M. Badescu, and X. Bao, "The ultrasonic/sonic driller/corer (usdc) as a subsurface drill, sampler and lab-on-a-drill for planetary exploration applications," 2005.
- [9] S. Thrun, M. Diel, and D. Hähnel, "Scan alignment and 3-d surface modeling with a helicopter platform," in *Field and Service Robotics*. Springer, 2003, pp. 287–297.
- [10] T. Templeton, D. H. Shim, C. Geyer, and S. S. Sastry, "Autonomous vision-based landing and terrain mapping using an mpc-controlled unmanned rotorcraft," in *Robotics and automation, 2007 IEEE international conference on*. IEEE, 2007, pp. 1349–1356.
- [11] P. Corke, S. Hrabar, R. Peterson, D. Rus, S. Saripalli, and G. Sukhatme, "Autonomous deployment and repair of a sensor network using an unmanned aerial vehicle," in *Robotics and Automation, 2004. Proceedings. ICRA'04. 2004 IEEE International Conference on*, vol. 4. IEEE, 2004, pp. 3602–3608.
- [12] K. S. Pister, "Tracking vehicles with a uav-delivered sensor network," 2001.
- [13] K. K. Millheim and M. E. Chenevert, *Applied drilling engineering*, vol. 2.
- [14] Y. Bar-Cohen and K. Zacny, *Drilling in extreme environments: penetration and sampling on earth and other planets*. John Wiley & Sons, 2009.
- [15] E. Detournay, T. Richard, and M. Shepherd, "Drilling response of drag bits: theory and experiment," *International Journal of Rock Mechanics and Mining Sciences*, vol. 45, no. 8, pp. 1347–1360, 2008.
- [16] D. D. Jones and M. F. Kocher, "Auger design for uniform unloading of granular material: I. rectangular cross-section containers," *Transactions of the ASAE*, vol. 38, no. 4, pp. 1157–1162, 1995.
- [17] K. Nagaoka, "Study on soil-screw interaction of exploration robot for surface and subsurface locomotion in soft terrain," *Graduate University for Advanced Studies (Sokendai), Hayama*, 2011.
- [18] B. M. Das, *Soil mechanics laboratory manual*. Oxford University Press New York, USA, 2002.
- [19] K. Terzaghi, R. B. Peck, and G. Mesri, *Soil mechanics in engineering practice*. John Wiley & Sons, 1996.
- [20] W. Lili, L. Zhiqian, W. Weiren, and Z. Zhijing, "Multi-objective optimization of drill stems motion parameter of lunar automatic drill sampling mechanism," *Journal of Astronautics*, vol. 36, no. 6, pp. 723–730, 2015.
- [21] K. Zacny, Y. Bar-Cohen, K. Davis, P. Coste, G. Paulsen, S. Sherrit, J. George, B. Derkowski, S. Gorevan, D. Boucher *et al.*, "Extraterrestrial drilling and excavation," *Drilling in Extreme Environments: Penetration and Sampling on Earth and other Planets*, pp. 347–557, 2009.
- [22] H. Rabia, "Specific energy as a criterion for drill performance prediction," in *International Journal of Rock Mechanics and Mining Sciences & Geomechanics Abstracts*, vol. 19, no. 1. Elsevier, 1982, pp. 39–42.